

Geodesic acoustic modes with poloidal mode couplings ad infinitum

Rameswar Singh¹, Ö D Gürçan¹, X Garbet², P Hennequin¹, L Vermare¹, P Morel¹ and R Singh³¹

¹*Laboratoire de Physique des Plasmas, Ecole Polytechnique, 91128 Palaiseau Cedex, France*

²*CEA, IRFM, F-13108 Saint Paul Lez Durance, France*

³*WCI, NFRI, Daejeon, Republic of Korea* ^{a)}

(Dated: October 10, 2018)

Geodesic acoustic modes (GAMs) are studied, for the first time, including all poloidal mode (m) couplings using drift reduced fluid equations. The nearest neighbor coupling pattern, due to geodesic curvature, leads to a semi-infinite chain model of the GAM with the mode-mode coupling matrix elements proportional to the radial wave number k_r . The infinite chain can be reduced to a renormalized bi-nodal chain with a matrix continued fractions. Convergence study of linear GAM dispersion with respect to k_r and the m -spectra confirms that high m couplings become increasingly important with k_r . The radially sorted roots overlap with experimentally measured GAM frequency profile in low collisionality shots in Tore Supra thus explaining the reduced frequency of GAM in Tore Supra.

Keywords: GAMs, poloidal mode couplings, matrix continued fractions, ITG turbulence, zonal flows

^{a)}Electronic mail: rameswar.singh@lpp.polytechnique.fr

I. INTRODUCTION

Control of turbulent transport is one of the key requirements for the improvement of the confinement time necessary for achieving controlled thermonuclear fusion. Large scale flow structures such as zonal flows¹ that are self-generated by, and that suppress the underlying micro turbulence and hence the turbulent transport in tokamaks by shearing the turbulent eddies², provide an important potentiality to this end. Geodesic acoustic modes (or GAMs), first predicted by Winsor *et al*³, are oscillating zonal flows, which also have a regulating effect on turbulence. While zonal flows are mostly stationary, GAM oscillations are sustained by geodesic curvature of the equilibrium magnetic field, which also allows them to be observed⁴⁻⁸. GAMs are linearly damped via Landau damping⁹, and thus exist mainly near the edge region, in a standard tokamak. They may be excited by non-linear Reynolds stresses¹⁰⁻¹⁶, poloidally asymmetric particle flux¹⁰ and heat fluxes¹⁷ and linearly by energetic particles¹⁸⁻²⁴.

Despite many progress in understanding of GAMs and their interaction with the underlying turbulence, even the linear structure of the GAM is still not perfectly understood. It is usually argued that the electrostatic GAM is made of toroidal mode $n = 0$, and poloidal mode number $m = 0$ of potential $\delta\phi$ and $n = 0$, $m = 1$ of density δn , temperature δT and parallel velocity δv_{\parallel} perturbations with $\sin\theta$ parity of $\delta n, \delta T$ and $\cos\theta$ parity of δv_{\parallel} in the poloidal direction. But it is well known in the study of toroidal drift waves that the magnetic curvature couples the poloidal mode numbers to their nearest neighbors making m a bad quantum number²⁵. GAM is no exception to this. These couplings are dropped usually beyond $m = 1$ or sometimes at $m = 2$ ^{14,26}.

This paper revisits the theory of GAM with poloidal mode couplings *ad-infinitum*. For simplicity and to bring out the novel effects, linear theory of GAMs are studied in a simple Ion temperature gradient driven (ITG) turbulence with adiabatic electron response using the drift reduced Braginskii equations^{27,28}, which may be suitable for the edge region of a modern day tokamak. The toroidal coupling of different poloidal modes that constitute the GAM appear as a nearest neighbor coupling of an infinite set of equations with appropriate parities in θ . A vector recurrence relation with appropriately defined orbitals leads to an elegant semi-infinite chain model of GAM, which can be reduced to a renormalized bi-nodal chain using a matrix continued fraction (MCF) approach²⁹. GAM dispersion at different

chain lengths shows that the high m couplings become more important with increasing k_r . Recently it was observed that the GAM frequency in Tore Supra is 50% smaller than the theoretical predictions from gyrokinetic model³⁰ and fluid models with effects of finite beta and collisionality and keeping only the poloidal mode numbers up to $m = 1$ ³¹. Our theoretical model is compared with the experimental GAM frequencies observed in Tore Supra shots and it is found that the experimental values of frequencies overlap with the radially sorted theoretical values of GAM frequencies when high poloidal mode couplings are retained.

The rest of the paper is organized as follows. In SectionII the drift reduced Braginskii equations are briefly discussed. Fully nonlinear electrostatic GAM equations are derived from drift reduced Braginskii equations in the SectionIII. Experimental comparisons are presented in SectionIV and the conclusions are drawn in SectionV.

II. DRIFT REDUCED BRAGINSKII EQUATIONS

We start with the electrostatic subset of the drift reduced fluid equations derived in Refs^{27,31} which were obtained from Braginskii equations²⁸. The space time scales are normalized as $r = r/\rho_s$, $\nabla_{\parallel} \equiv L_n \nabla_{\parallel}$, $t = tc_s/L_n$. The perturbed field quantities are normalized to their mixing length levels: $\phi = (e\delta\phi/T_{e0})(L_n/\rho_s)$, $n_i = (\delta n_i/n_0)(L_n/\rho_s)$, $v = (\delta v_{\parallel i}/c_s)(L_n/\rho_s)$, $p_i = (\delta p_i/P_{e0})(L_n/\rho_s)$. The remaining dimensionless parameters are : $\eta_i = L_{n_{i0}}/L_{T_{i0}}$, $\varepsilon_n = 2L_n/R$, $K = \tau_i(1 + \eta_i)$, $\tau_i = T_{i0}/T_{e0}$, $\rho_s = c_s/\omega_{ci}$ is ion Larmor radius, and $c_s = \sqrt{T_{e0}/m_i}$ is ion sound speed where m_i is ion mass. The nonlinearities in the following equations originates mainly from $E \times B$ drift nonlinearity i.e., $\vec{v}_{E \times B} \cdot \vec{\nabla} f = [\phi, f]$, and polarization drift nonlinearity $\vec{v}_{E \times B} \cdot \vec{\nabla} \nabla_{\perp}^2 f = [\phi, \nabla_{\perp}^2 f]$.

A. Electron response

In the collisionless limit the electron temperature perturbations are washed out $T_e = 0$. Then assuming the limit $\omega \ll k_{\parallel} c_s$ the parallel electron momentum equation yields the adiabatic electron response

$$n_e = \phi \tag{1}$$

B. Ion response

The perturbed ion density equation is given by

$$\begin{aligned} \frac{\partial n_i}{\partial t} + \frac{1}{r} \frac{\partial \phi}{\partial \theta} - \varepsilon_n \left(\cos \theta \frac{1}{r} \frac{\partial}{\partial \theta} + \sin \theta \frac{\partial}{\partial r} \right) (\phi + \tau_i n_i + \tau_i T_i) - \left(\frac{\partial}{\partial t} - K \frac{1}{r} \frac{\partial}{\partial \theta} \right) \nabla_{\perp}^2 \phi \\ + \nabla_{\parallel} v_{\parallel} = - [\phi, n_i] + \vec{\nabla} \cdot [\phi + p_i, \vec{\nabla}_{\perp} \phi] \end{aligned} \quad (2)$$

Here the second term on the left hand side is the $E \times B$ convection of equilibrium density, the third term comes from divergence of the $E \times B$ velocity plus the divergence of diamagnetic particle flux, the fourth term comes from the divergence of the polarization drift and the fifth term simply represents the parallel compression. On the right hand side, the first term is the $E \times B$ nonlinearity and the second term is polarization nonlinearity. The Poisson brackets are defined as $[a, b] = \frac{\partial a}{\partial r} \frac{1}{r} \frac{\partial b}{\partial \theta} - \frac{1}{r} \frac{\partial a}{\partial \theta} \frac{\partial b}{\partial r}$. Here r, θ, φ represent the radial, poloidal and toroidal coordinates in tokamak and circular flux surfaces are assumed for the equilibrium. The equilibrium magnetic field is given by $\vec{B} = B_{\varphi}(\vec{e}_{\varphi} + \frac{r}{qR}\vec{e}_{\theta})$ where the toroidal magnetic field is $B_{\varphi} = \frac{B_0}{1+(r/R_0)\cos\theta}$. Adding the electron momentum equation to the ion momentum equation and then using the electron temperature equation, the parallel ion velocity equation becomes:

$$\begin{aligned} \frac{\partial v_{\parallel}}{\partial t} - 2\tau_i \varepsilon_n \left(\cos \theta \frac{1}{r} \frac{\partial}{\partial \theta} + \sin \theta \frac{\partial}{\partial r} \right) v_{\parallel} + \nabla_{\parallel} [\tau_i n_i + \tau_i T_i + \phi] \\ = - [\phi, v_{\parallel}] + n_i \nabla_{\parallel} p_i \end{aligned} \quad (3)$$

The second term on the left hand side originates in parts from the divergence of ion stress tensor after the gyroviscous cancellation. The third term represents the sum of parallel pressure and electric force. The first term on the right hand side is the $E \times B$ nonlinearity and second term is the parallel pressure force nonlinearity. The ion temperature equation reads

$$\begin{aligned} \frac{\partial}{\partial t} \left(T_i - \frac{2}{3} n_i \right) - \frac{5}{3} \varepsilon_n \left(\cos \theta \frac{1}{r} \frac{\partial}{\partial \theta} + \sin \theta \frac{\partial}{\partial r} \right) T_i + \left(\eta_i - \frac{2}{3} \right) \frac{1}{r} \frac{\partial \phi}{\partial \theta} \\ = -\sqrt{2\tau_i} |\nabla_{\parallel}| T_i - \left[\phi, T_i - \frac{2}{3} n_i \right] \end{aligned} \quad (4)$$

The second term on the left hand side originates from the divergence of diamagnetic heat flux after cancellation in parts with diamagnetic convection of heat. The first term on the right hand side represents Landau damping à la Hammet and Perkins³². The second term on

the right represents nonlinear $E \times B$ convection of heat. Finally the quasineutrality $n_e = n_i$ is used for the perturbations in the form of the vorticity equation

$$\begin{aligned} & \left(\frac{\partial}{\partial t} - K \frac{1}{r} \frac{\partial}{\partial \theta} \right) \nabla_{\perp}^2 \phi + \varepsilon_n \left(\cos \theta \frac{1}{r} \frac{\partial}{\partial \theta} + \sin \theta \frac{\partial}{\partial r} \right) [\tau_i n_i + \tau_i T_i + n_e] \\ & = -\vec{\nabla} \cdot \left[\phi + p_i, \vec{\nabla}_{\perp} \phi \right] \end{aligned} \quad (5)$$

The first term on the left hand side is the divergence of polarization current and the second term is the divergence of diamagnetic current. The term on the right hand side is the polarization nonlinearity.

III. ELECTROSTATIC COLLISIONLESS GEODESIC ACOUSTIC MODES

In the minimal description, the GAM is said to be made of poloidally smooth potential and $\sin \theta$ parity of density perturbations. However here we wish to derive the equations for GAM with all poloidal mode couplings. Hence we start by taking the flux surface average of the vorticity equation.

$$\frac{\partial}{\partial t} \nabla_r^2 \langle \phi \rangle + \varepsilon_n \nabla_r [(1 + \tau_i) \langle n \sin \theta \rangle + \tau_i \langle T_i \sin \theta \rangle] = - \left\langle \vec{\nabla} \cdot \left[\phi + p_i, \vec{\nabla}_{\perp} \phi \right] \right\rangle \quad (6)$$

The angular bracket represents flux surface averaging defined by $\langle (\dots) \rangle = \int r d\theta d\varphi (\dots) / \int r d\theta d\varphi$. The nonlinear term on the right hand side represents the divergence of vorticity flux and is attributed to turbulent excitation of GAM¹¹. This shows the need for an equation for $\langle n \sin \theta \rangle$ which is obtained by multiplying the ion continuity equation by $\sin \theta$ followed by flux surface average. In the following a general equation for poloidal mode number m for $\langle n \sin m\theta \rangle$ is obtained.

$$\begin{aligned} & \frac{\partial}{\partial t} \langle n \sin m\theta \rangle - \frac{\partial}{\partial t} \nabla_r^2 \langle \phi \sin m\theta \rangle - \frac{\varepsilon_n}{2} \nabla_r [\langle \phi \cos(m-1)\theta \rangle + \tau_i \langle n \cos(m-1)\theta \rangle] \\ & + \tau_i \langle T_i \cos(m-1)\theta \rangle - \langle \phi \cos(m+1)\theta \rangle - \tau_i \langle n \cos(m+1)\theta \rangle - \tau_i \langle T_i \cos(m+1)\theta \rangle \\ & - \frac{\varepsilon_n}{2q} m \langle v_{\parallel} \cos m\theta \rangle = - \left\langle \vec{\nabla} \cdot \left[\phi + p_i, \vec{\nabla}_{\perp} \phi \right] \sin m\theta \right\rangle + \langle S_n \sin m\theta \rangle \end{aligned} \quad (7)$$

The first term on the right hand side is the $\sin m\theta$ weighted flux surface averaged divergence of vorticity flux. The second term represents θ antisymmetric part of the particle source S_n . This then shows the need for the equation for $\langle v_{\parallel} \cos m\theta \rangle$, which is obtained by multiplying

the parallel ion velocity equation (3) by $\cos m\theta$ followed by flux surface average

$$\begin{aligned} & \frac{\partial}{\partial t} \langle v_{\parallel} \cos m\theta \rangle - \tau_i \varepsilon_n \nabla_r [\langle v_{\parallel} \sin(m+1)\theta \rangle - \langle v_{\parallel} \sin(m-1)\theta \rangle] \\ & + \frac{\varepsilon_n}{2q} m [(1 + \tau_i) \langle n \sin m\theta \rangle + \tau_i \langle T_i \sin m\theta \rangle] = - \langle [\phi, v_{\parallel}] \cos m\theta \rangle \\ & + \langle (n \nabla_{\parallel} (p_i + n)) \cos m\theta \rangle + \langle S_v \cos m\theta \rangle \end{aligned} \quad (8)$$

The various nonlinear terms on the right hand side of the above equation can be identified as follows: The first term coming from the $E \times B$ convective nonlinearity is the $\cos m\theta$ weighted, flux surface averaged, divergence of the parallel velocity flux. The second term is the flux surface average of the turbulent parallel acceleration weighted by $\cos m\theta$. This term survives only when there is a k_{\parallel} symmetry breaking mechanism present³³, which breaks the dipolar structure of acceleration in θ . The last term is the θ symmetric part of the external velocity/ momentum source S_v . Similarly the equation for $\langle T_i \sin m\theta \rangle$ is obtained by multiplying the ion temperature equation by $\sin m\theta$ followed by flux surface average

$$\begin{aligned} & \frac{\partial}{\partial t} \left(\langle T_i \sin m\theta \rangle - \frac{2}{3} \langle n \sin m\theta \rangle \right) - \frac{5}{3} \frac{\varepsilon_n}{2} \nabla_r [\langle T_i \cos(m-1)\theta \rangle - \langle T_i \cos(m+1)\theta \rangle] \\ & = -\sqrt{2\tau_i} \frac{\varepsilon_n}{2q} m \langle T_i \sin m\theta \rangle - \left\langle \left[\phi, T_i - \frac{2}{3} n \right] \sin m\theta \right\rangle + \langle S_T \sin m\theta \rangle \end{aligned} \quad (9)$$

where the first term on the right hand side represents Landau damping á la Hammett-Perkins³², the second term is the $\sin m\theta$ weighted flux surface averaged divergence of heat flux which has been shown to excite GAM for $m = 1$ ¹⁷. And the third term represents the θ antisymmetric part of the heat source S_T . The above equations are supplemented by the adiabatic electron response, which can be written as:

$$\langle n \sin m\theta \rangle = \langle \phi \sin m\theta \rangle \quad (10)$$

These equations show that the perturbations with sine/cosine parity and the poloidal mode number m are coupled to those with the poloidal mode numbers $m+1$, $m-1$ and cosine/sine parity. Hence we write the equations for $m+1$ (flipping the parity):

$$\begin{aligned} & \frac{\partial}{\partial t} \langle n \cos(m+1)\theta \rangle - \frac{\partial}{\partial t} \nabla_r^2 \langle \phi \cos(m+1)\theta \rangle - \frac{\varepsilon_n}{2} \nabla_r [\langle \phi \sin(m+2)\theta \rangle + \tau_i \langle n \sin(m+2)\theta \rangle] \\ & + \tau_i \langle T_i \sin(m+2)\theta \rangle - \langle \phi \sin m\theta \rangle - \tau_i \langle n \sin m\theta \rangle - \tau_i \langle T_i \sin m\theta \rangle] + \frac{\varepsilon_n}{2q} (m+1) \langle v_{\parallel} \sin(m+1)\theta \rangle \\ & = - \left\langle \vec{\nabla} \cdot \left[\phi + p_i, \vec{\nabla}_{\perp} \phi \right] \cos(m+1)\theta \right\rangle + \langle S_n \cos(m+1)\theta \rangle \end{aligned} \quad (11)$$

$$\begin{aligned}
& \frac{\partial}{\partial t} \langle v_{\parallel} \sin(m+1)\theta \rangle - \tau_i \varepsilon_n \nabla_r [\langle v_{\parallel} \cos m\theta \rangle - \langle v_{\parallel} \cos(m+2)\theta \rangle] \\
& - \frac{\varepsilon_n}{2q} (m+1) [(1+\tau_i) \langle n \cos(m+1)\theta \rangle + \tau_i \langle T_i \cos(m+1)\theta \rangle] \\
& = - \langle [\phi, v_{\parallel}] \sin(m+1)\theta \rangle + \langle (n \nabla_{\parallel} (p_i + n)) \sin(m+1)\theta \rangle + \langle S_v \sin(m+1)\theta \rangle \quad (12)
\end{aligned}$$

$$\begin{aligned}
& \frac{\partial}{\partial t} \left(\langle T_i \cos(m+1)\theta \rangle - \frac{2}{3} \langle n \cos(m+1)\theta \rangle \right) - \frac{5\varepsilon_n}{3} \nabla_r [\langle T_i \sin(m+2)\theta \rangle - \langle T_i \sin m\theta \rangle] \\
& = -\sqrt{2\tau_i} \frac{\varepsilon_n}{2q} (m+1) \langle T_i \cos(m+1)\theta \rangle - \left\langle \left[\phi, T_i - \frac{2}{3}n \right] \cos(m+1)\theta \right\rangle \quad (13) \\
& + \langle S_T \cos(m+1)\theta \rangle
\end{aligned}$$

$$\frac{\partial}{\partial t} \langle T_i \rangle - \frac{5\varepsilon_n}{3} \nabla_r \langle T_i \sin \theta \rangle = - \langle [\phi, T_i] \rangle + \langle S_{T_i} \rangle \quad (14)$$

$$\langle n \cos(m+1)\theta \rangle = \langle \phi \cos(m+1)\theta \rangle \quad (15)$$

In the above equations S_n , S_T and S_v represents particle, heat and momentum sources respectively. For $m = 1, 3, 5, \dots$ etc., the above set of equations yield an infinite set of equations that describe a GAM in its full glory with all the nonlinearities and external sources. Hence the GAM oscillations in general appear as a result of the linear coupling of $\langle (\phi, T) \rangle$, $\langle (n, \phi, T) \sin m\theta \rangle$, $\langle (n, \phi, T) \cos(m+1)\theta \rangle$, $\langle v_{\parallel} \cos m\theta \rangle$, $\langle v_{\parallel} \sin(m+1)\theta \rangle$. It is apparent from the above set of equations that not just the poloidal Reynolds stress and $\sin \theta$ component of heat flux but all poloidal harmonics of poloidal Reynolds stress, parallel Reynolds stress, parallel acceleration, heat flux and all poloidal harmonics of particle, momentum and heat sources act as source/sink of GAM excitation/damping. A detailed investigation of the role of different poloidal harmonics of turbulent particle, momentum and heat fluxes; and different poloidal harmonics of external sources of particle, momentum and heat sources will be presented elsewhere. In this paper we proceed to present the linear dynamics with poloidal mode coupling ad infinitum.

Compact representation:- These equations in general can be written as a nonlinear matrix equation of infinite dimension in the following form

$$\frac{\partial G}{\partial t} = MG + N + S \quad (16)$$

where

$$G = (G_0, G_1, G_2, G_3, \dots)^\dagger \quad (17)$$

Taking $G \propto e^{\lambda t}$, the equations of the orbitals become

$$\alpha G_1 = \lambda G_0 \quad (21)$$

$$\beta G_0 + A_1 G_1 + B G_2 = \lambda G_1 \quad (22)$$

$$\begin{aligned} & -(-1)^{m-1} B G_{m-1} + m A_m G_m \\ & + (-1)^{m+1} B G_{m+1} = \lambda G_m \end{aligned} \quad (23)$$

where $m = 2, 3, 4, \dots$, and $A_m = \begin{cases} A^+ & ; m = 1, 3, 5, \dots \\ A^- & ; m = 2, 4, 6, \dots \end{cases}$. A graphical representation of

the above equations shows that these orbitals form a semi-infinite chain as shown in Fig. (1), where the orbitals are represented by vertices(nodes) and the couplings are represented by the edges connecting the vertices. More detailed couplings are shown in Fig. (2) where the edges in red color represents the self-coupling due to Landau damping.

Matrix Continued Fraction (MCF): Equations (22) onwards can be reduced to a single equation relating G_0 and G_1 via a matrix continued fraction(MCF) equation as follows:

$$\begin{aligned} \beta G_0 &= \left\{ (\lambda - A^+) - B \left[\lambda - 2A^- - B \left[\lambda - 3A^+ - B \left[\lambda - 4A^- - \dots \right]^{-1} B \right]^{-1} B \right]^{-1} B \right\} G_1 \\ &= \kappa(\lambda) G_1 \end{aligned} \quad (24)$$

This amounts to renormalization of coupling matrix β to $\kappa^{-1}\beta$. Now the equations (21) and (24) can be combined to get a reduced matrix equation:

$$\begin{bmatrix} \lambda & -\alpha \\ -\beta & \kappa(\lambda) \end{bmatrix} \begin{bmatrix} G_0 \\ G_1 \end{bmatrix} = 0 \quad (25)$$

for which the eigenvalues λ can be obtained from the condition:

$$\begin{vmatrix} \lambda & -\alpha \\ -\beta & \kappa(\lambda) \end{vmatrix} = 0$$

The existence of κ means that the infinite chain can be reduced to a renormalized binodal chain as shown in figure(1). In this picture the minimal description of GAM is obtained when the infinite chain is terminated at $m = 1$ i.e., the binodal chain. This binodal chain has

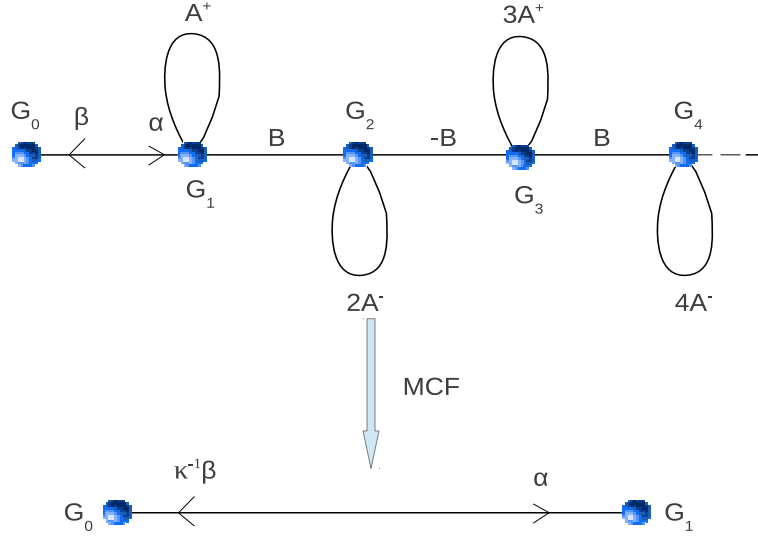


Figure 1. 1d chain model of GAM

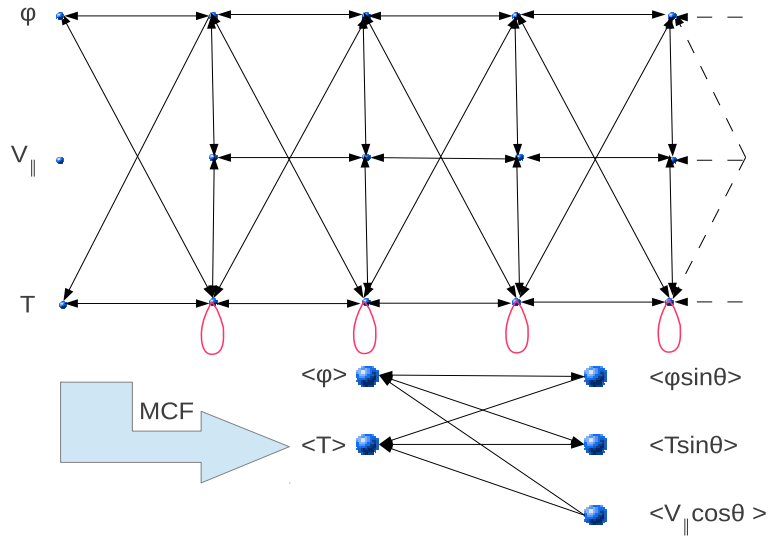


Figure 2. Zoom-in of FIG.1

5 roots. In general a chain terminated at the m^{th} node has $3m + 2$ roots. So the infinitely extended chain has infinite number of roots. But the fact that the infinite chain can be reduced to a renormalized binodal chain which again has only 5 roots means that only 5 roots are physical out of the infinite number of roots of the infinitely extended chain.

IV. NUMERICAL SOLUTIONS AND COMPARISON WITH EXPERIMENTS

A. Eigenvalues and amplitude spectra

In the absence of an analytical form for the MCF κ , the matrix M is solved numerically for its eigenvalues and eigenvectors by terminating the chain at different orbitals or m values. *Root sorting algorithm:* For $k_r = 0$ the intermodal coupling matrix B becomes a null matrix and the intermodal coupling beyond $m > 1$ vanishes. This means for closure at any m the physical roots are the ones which has the same values as the roots for $k_r = 0$ at $m = 1$ closure i.e., $\lambda(k_r = 0, m = 1) = \lambda_i(k_r = 0, m = m)$. Then the correct physical dispersion branch is followed by minimizing λ in k_r i.e., minimizing $|\lambda_i(k_r) - \lambda_j(k_r + \Delta k_r)|$.

Frequency: FIG.(3) shows the radial wave number dispersion of GAM frequency, with and without Landau damping, when the chain is terminated at different nodes for the parameters $\tau_i = 1$ and $q = 4$. The dispersion curve converges at $m \geq 2$ towards low k_r and and at $m \geq 14$ towards high k_r . This clearly means that the number of orbitals needed for convergence increases with k_r . It is also clearly seen that Landau damping has strong effect on the converged GAM dispersion at and beyond moderately high k_r values which dramatically changes the radial group propagation properties of GAM.

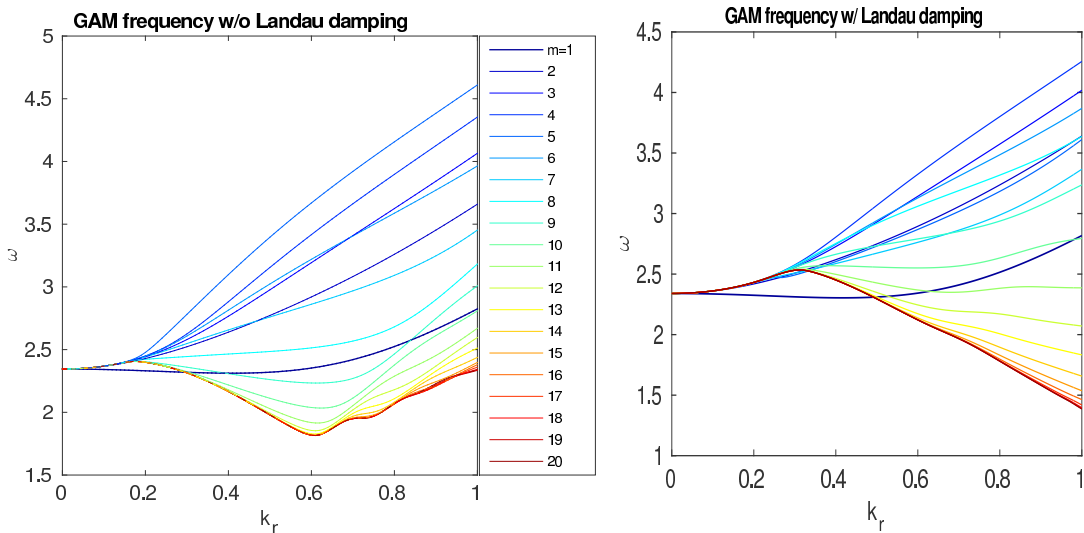


Figure 3. GAM dispersion convergence with increasing m . Left: GAM frequency without Landau damping. Right: GAM frequency with Landau damping. Parameters: $\tau_i = 1$, $q = 4$.

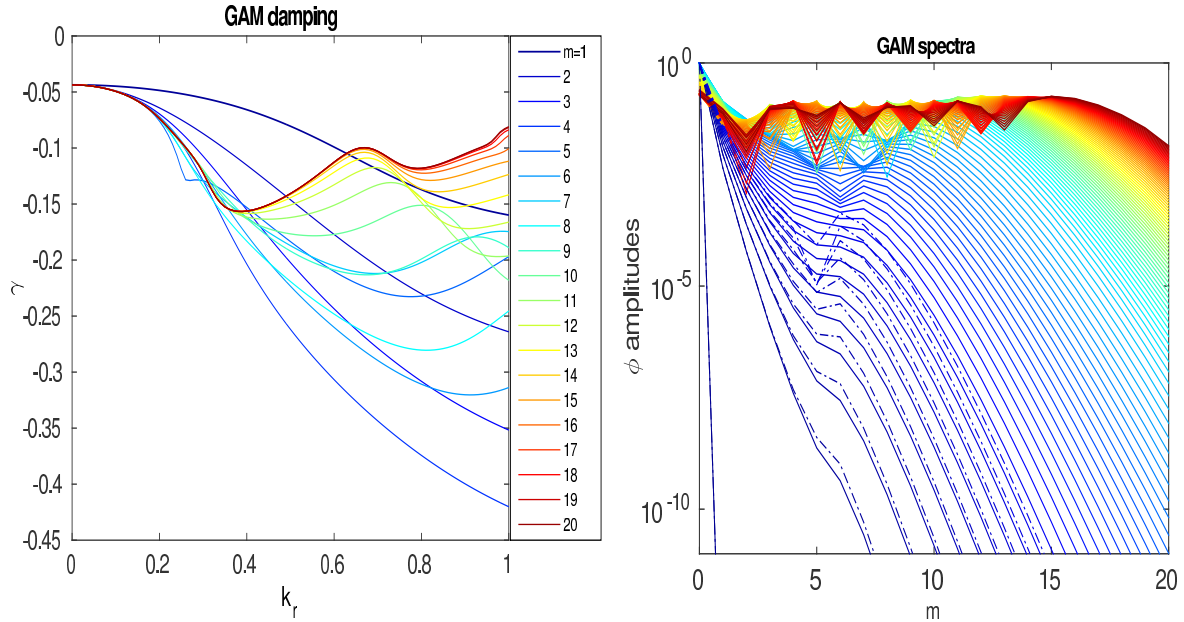


Figure 4. Left: GAM Landau damping. Right: GAM spectra of ϕ in (m, k_r) . Color coding: Blue to red $k_r = [0 : 0.01 : 1]$. Dotted lines represent amplitude spectra without Landau damping.

The radial group velocity can be positive, zero or negative depending on the value of k_r and Landau damping effect.

Damping and amplitude spectra: The damping and amplitude spectra also confirms the same features. The left side of figure (4) shows that the converged damping curve is very much different from the damping at closure $m = 1$. The amplitude spectra in m is plotted for different values of k_r in figure(4). The amplitude spectra shows that the amplitude increases with k_r at any poloidal mode number m . At any k_r the amplitude decreases rapidly with m . Also the amplitude without Landau damping effect is slightly higher than that with Landau damping. All this conveys the same consistent lesson that poloidal mode coupling becomes important with k_r .

B. Experimental comparison

Equilibrium profiles: The equilibrium profiles for the two different collisionality shots of Tore Supra³⁴ are shown in the figure(5). The shot number #45511 is a low temperature high collisionality shot and the shot number #45494 is a high temperature low collisionality shot where densities and the safety factors are almost same in both shots.

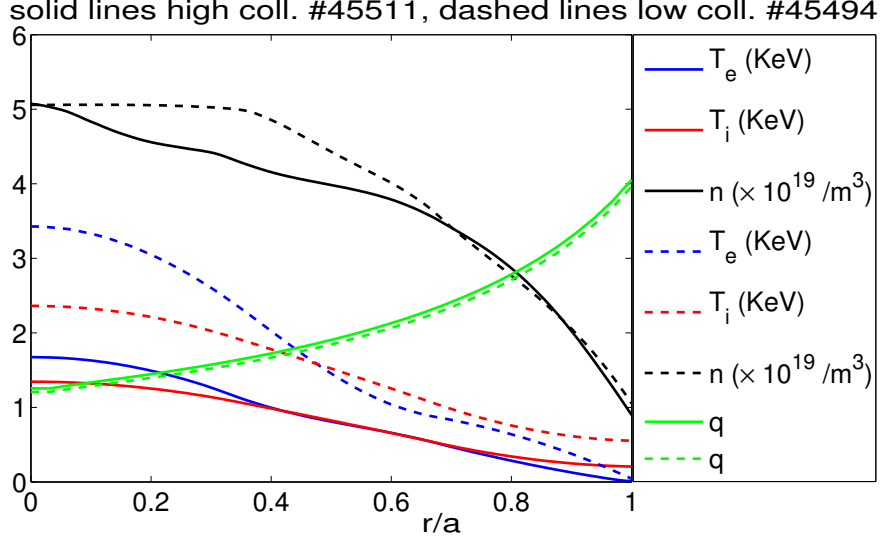


Figure 5. Equilibrium profiles of Tore Supra

Root sorting and experiment-theory comparison: For the given equilibrium profiles the roots can be sorted either in radial wave number k_r at each radial location r as described in the previous subsection or it can be sorted in r at each k_r . Radial sorting is done by first obtaining the roots at $r = 0$ by k_r sorting. Then $|\lambda_i(r) - \lambda_j(r + \Delta r)|$ is minimized with respect to r to follow the roots smoothly in radius. The k_r sorted roots display discontinuous jumps in radial profile for $k_r > 0.1$ as can be seen in the top panels of figures(6) and (7). The experimentally measured frequencies are however almost 50% below the theoretically obtained k_r sorted roots. The radially sorted roots on the other hand, jumps in the k_r space as can be seen in the bottom panels of the figures (6) and (7). The experimental GAM frequencies overlap with the theoretical r sorted frequencies for the low collisionality shot in the range $0.1 < k_r < 0.15$ as shown in the bottom pannel of figure(6). However for the high collisionality shot, the experimental values fail to overlap with the theoretical r sorted roots and falls in the spectral gap, see bottom panel of figure(7). This may be a reflection of the fact that the effects of collision are not correctly captured by our theoretical model.

V. CONCLUSIONS

In conclusions we presented the most general picture of GAMs in tokamak in the fluid theoretical framework starting from the Braginskii equations applied to ITG turbulence.

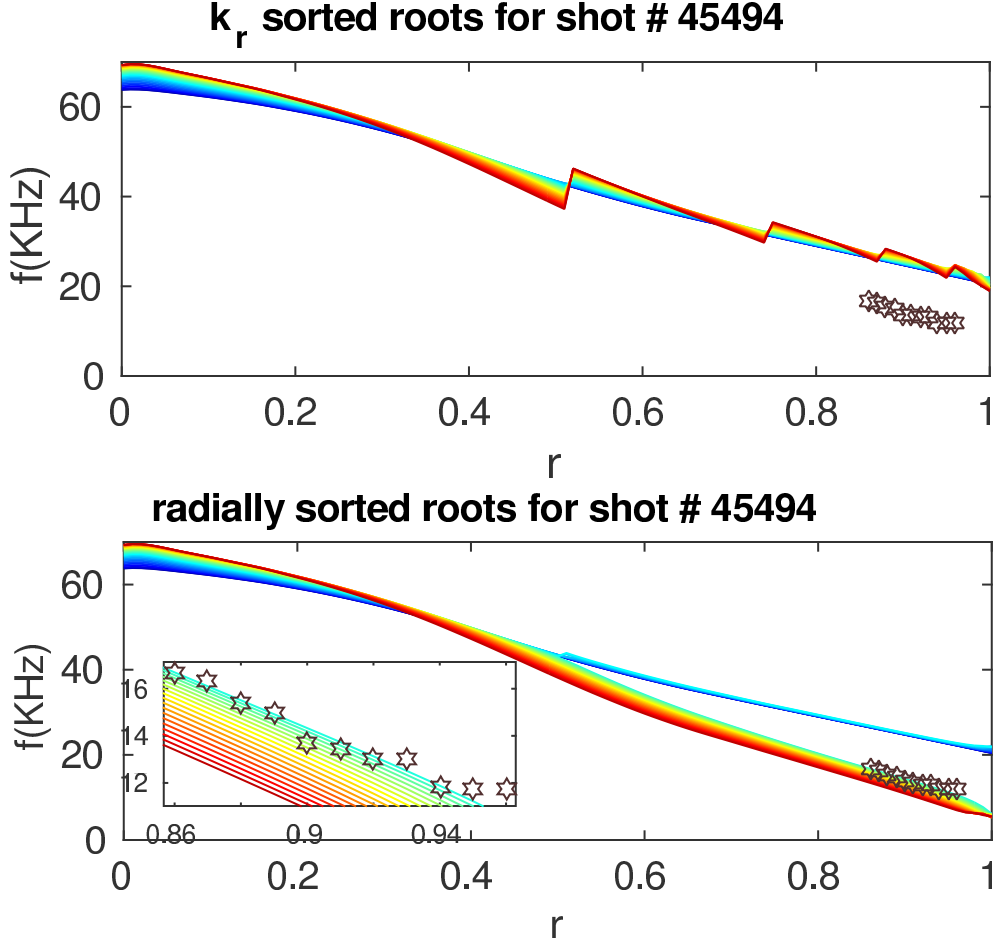


Figure 6. Experiment theory comparison of GAM frequency for low collisionality shot. Top: k_r sorted roots. Bottom: Radially sorted roots. Color coding: blue to red $k_r = [0 : 0.01 : 0.3]$. Closure at $m = 15$ is used for all calculations. The stars are the experimentally measured GAM frequencies.

The unique feature of the model is that it retains poloidal mode couplings ad infinitum which allows to study the effects of higher poloidal mode couplings in a systematic manner. Because of geodesic curvature each poloidal mode m is coupled to its nearest neighbors $m + 1$ and $m - 1$ and hence infinite number of equations are required to describe a GAM. With appropriately defined sub-vectors of perturbations for poloidal mode m , dubbed here as orbitals, the infinite set of scalar equations become infinite set of vector equations with m^{th} orbital coupled to $m \pm 1$ orbitals. This leads to a semi-infinite $1d$ chain model of GAM with each node represented by an orbital. This infinite chain is reduced to a bi-nodal chain with renormalized coupling coefficients by use of a matrix continued fraction. Since an analytical

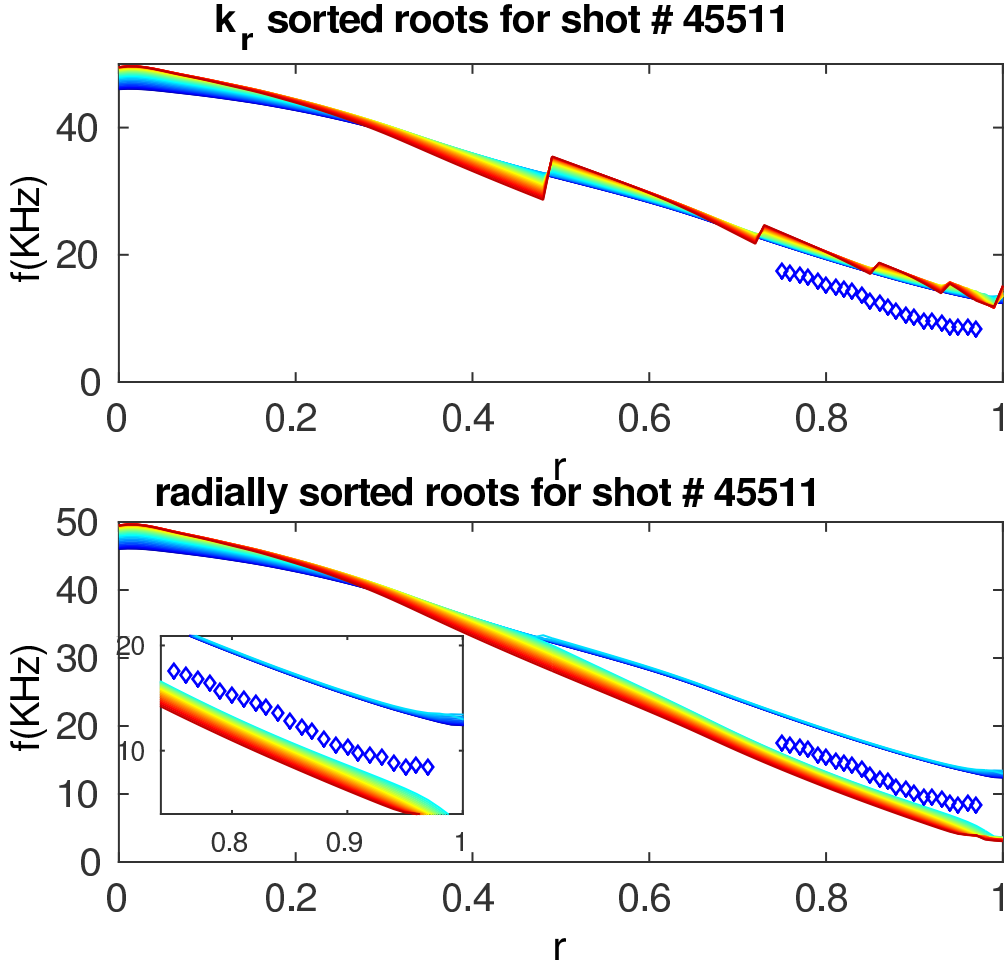


Figure 7. Experiment theory comparison of GAM frequency for high collisionality shot. Top: k_r sorted roots. Bottom: Radially sorted roots. Color coding: blue to red $k_r = [0 : 0.01 : 0.3]$. Closure at $m = 15$ is used for all calculations. The diamonds are the experimentally measured GAM frequencies.

form of the matrix continued fraction is not available, numerical methods are adopted to the dispersion, damping and mode amplitude properties by terminating the chain at different lengths. The main results of this paper are outlined below.

The GAM dispersion, damping at different chain lengths show that they converge with increasing chain lengths, the rate of convergence being faster at low k_r and slower at high k_r meaning that poloidal mode couplings are increasingly important with increasing k_r . The poloidal coupling beyond $m = 1$ vanishes at $k_r = 0$. These results are also supported from the linear amplitude spectra of potential in m with k_r as a parameter. The amplitudes of

perturbations beyond $m > 1$ increases with k_r showing that high m mode couplings become more important with k_r .

The theoretical results are compared with experimental observations of GAM frequency in Tore Supra. The frequencies sorted in k_r show discontinuous jumps in the radial profile of frequencies and the frequencies sorted in radial coordinate show discontinuous jumps in k_r . It is seen that radially sorted theoretical frequencies overlap well with the experimental frequencies in the low collisionality shot.

Though this is the most general theory for the description of GAM in a fluid theoretical framework, it is not free of weaknesses and assumptions and hence has further scope for improvements. For example it does not consider the diamagnetic and normal curvature effects which is justified for very low m closures only. For high m closure these effects become important. Such a work is in progress and will be presented elsewhere. Hammet-Perkins closure has been used to mimic the Landau damping in fluid model which is strictly valid for high m perturbations only. A gyrokinetic formulation of infinite poloidal mode coupling in GAM is desirable and is left as a future work.

ACKNOWLEDGMENTS

The authors are thankful to Y Sarazin, and G Dif-Paradalier, T.S. Hahm and P.H. Diamond for fruitful discussions. Thanks to A Storelli for providing the experimental profiles in Tore Supra. This work has been supported by funding from the “Departement D’Enseignement-Recherche de Physique Ecole Polytechnique” and it has been carried out within the framework of the EUROfusion Consortium and has received funding from the European Union’s Horizon 2020 research and innovation programme under grant agreement number 633053. This work was also partly supported by the french “Agence National de la Recherche” contract ANR JCJC 0403 01. The views and opinions expressed herein do not necessarily reflect those of the European Commission.

REFERENCES

- ¹Z. Lin, T. S. Hahm, W. W. Lee, W. M. Tang, and R. B. White, *Science* **281**, 1835 (1998).
- ²P. H. Diamond, S.-I. Itoh, K. Itoh, and T. S. Hahm, *Plasma. Phys. Cont* **47**, R35 (2005).

- ³N. Winsor, J. L. Johnson, and J. M. Dawson, *Physics of Fluids* **11**, 2448 (1968).
- ⁴M. Jakubowski, R. J. Fonck, and G. R. McKee, *Phys. Rev. Lett.* **89**, 265003 (Dec 2002), <http://link.aps.org/doi/10.1103/PhysRevLett.89.265003>.
- ⁵Y. Nagashima, K. Hoshino, A. Ejiri, K. Shinohara, Y. Takase, K. Tsuzuki, K. Uehara, H. Kawashima, H. Ogawa, T. Ido, Y. Kusama, and Y. Miura, *Phys. Rev. Lett.* **95**, 095002 (Aug 2005), <http://link.aps.org/doi/10.1103/PhysRevLett.95.095002>.
- ⁶A. Krämer-Flecken, S. Soldatov, H. R. Koslowski, and O. Zimmermann (TEXTOR Team), *Phys. Rev. Lett.* **97**, 045006 (Jul 2006), <http://link.aps.org/doi/10.1103/PhysRevLett.97.045006>.
- ⁷K. J. Zhao, T. Lan, J. Q. Dong, L. W. Yan, W. Y. Hong, C. X. Yu, A. D. Liu, J. Qian, J. Cheng, D. L. Yu, Q. W. Yang, X. T. Ding, Y. Liu, and C. H. Pan, *Phys. Rev. Lett.* **96**, 255004 (Jun 2006), <http://link.aps.org/doi/10.1103/PhysRevLett.96.255004>.
- ⁸L. Vermare, P. Hennequin, O. D. Gurcan, and the Tore Supra Team, *Nuclear Fusion* **52**, 063008 (2012), <http://stacks.iop.org/0029-5515/52/i=6/a=063008>.
- ⁹H. SUGAMA and T.-H. WATANABE, *Journal of Plasma Physics* **72**, 825 (12 2006), ISSN 1469-7807, http://journals.cambridge.org/article_S0022377806004958.
- ¹⁰K. Itoh, K. Hallatschek, and S.-I. Itoh, *Plasma Physics and Controlled Fusion* **47**, 451 (2005), <http://stacks.iop.org/0741-3335/47/i=3/a=004>.
- ¹¹N. Chakrabarti, R. Singh, P. K. Kaw, and P. N. Guzdar, *Physics of Plasmas* **14**, 052308 (2007), <http://scitation.aip.org/content/aip/journal/pop/14/5/10.1063/1.2732167>.
- ¹²N. Chakrabarti, P. N. Guzdar, R. G. Kleva, V. Naulin, J. J. Rasmussen, and P. K. Kaw, *Physics of Plasmas* **15**, 112310 (2008), <http://scitation.aip.org/content/aip/journal/pop/15/11/10.1063/1.3028311>.
- ¹³P. N. Guzdar, N. Chakrabarti, R. Singh, and P. K. Kaw, *Plasma Physics and Controlled Fusion* **50**, 025006 (2008), <http://stacks.iop.org/0741-3335/50/i=2/a=025006>.
- ¹⁴F. Zonca and L. Chen, *EPL (Europhysics Letters)* **83**, 35001 (2008), <http://stacks.iop.org/0295-5075/83/i=3/a=35001>.
- ¹⁵P. N. Guzdar, R. G. Kleva, N. Chakrabarti, V. Naulin, J. J. Rasmussen, P. K. Kaw, and R. Singh, *Physics of Plasmas* **16**, 052514 (2009), <http://scitation.aip.org/content/aip/journal/pop/16/5/10.1063/1.3143125>.
- ¹⁶L. Chen, Z. Qiu, and F. Zonca, *EPL (Europhysics Letters)* **107**, 15003 (2014), <http://stacks.iop.org/0295-5075/107/i=1/a=15003>.

- ¹⁷K. Hallatschek and D. Biskamp, Phys. Rev. Lett. **86**, 1223 (Feb 2001), <http://link.aps.org/doi/10.1103/PhysRevLett.86.1223>.
- ¹⁸G. Y. Fu, Phys. Rev. Lett. **101**, 185002 (Oct 2008), <http://link.aps.org/doi/10.1103/PhysRevLett.101.185002>.
- ¹⁹G. Y. FU, Journal of Plasma Physics **77**, 457 (8 2011), ISSN 1469-7807, http://journals.cambridge.org/article_S0022377810000619.
- ²⁰Z. Qiu, F. Zonca, and L. Chen, Plasma Physics and Controlled Fusion **52**, 095003 (2010), <http://stacks.iop.org/0741-3335/52/i=9/a=095003>.
- ²¹Z. Qiu, F. Zonca, and L. Chen, Physics of Plasmas **19**, 082507 (2012), <http://scitation.aip.org/content/aip/journal/pop/19/8/10.1063/1.4745191>.
- ²²D. Zarzoso, X. Garbet, Y. Sarazin, R. Dumont, and V. Grandgirard, Physics of Plasmas **19**, 022102 (2012), <http://scitation.aip.org/content/aip/journal/pop/19/2/10.1063/1.3680633>.
- ²³L. Wang, J. Q. Dong, Z. He, H. He, and Y. Shen, Physics of Plasmas **21**, 072511 (2014), <http://scitation.aip.org/content/aip/journal/pop/21/7/10.1063/1.4890467>.
- ²⁴J.-B. Girardo, D. Zarzoso, R. Dumont, X. Garbet, Y. Sarazin, and S. Sharapov, Physics of Plasmas **21**, 092507 (2014), <http://scitation.aip.org/content/aip/journal/pop/21/9/10.1063/1.4895479>.
- ²⁵W. Horton, R. Estes, H. Kwak, and D. Choi, Physics of Fluids **21** (1978).
- ²⁶C. Nguyen, X. Garbet, and A. I. Smolyakov, Physics of Plasmas **15**, 112502 (2008), <http://scitation.aip.org/content/aip/journal/pop/15/11/10.1063/1.3008048>.
- ²⁷A. Zeiler, J. F. Drake, and B. Rogers, Physics of Plasmas **4** (1997).
- ²⁸S. I. Braginskii, Reviews of Plasma Physics edited by M. A. Leontovich **I**, 205 (1965).
- ²⁹H. Risken, *The Fokker-Planck Equation: Methods of Solution and its Applications* (Springer, 1989).
- ³⁰A. Storelli, L. Vermare, P. Hennequin, O. D. Gurcan, G. Dif-Pradalier, Y. Sarazin, X. Garbet, T. Gorler, R. Singh, P. Morel, V. Grandgirard, P. Ghendrih, and T. S. team, Physics of Plasmas **22**, 062508 (2015), <http://scitation.aip.org/content/aip/journal/pop/22/6/10.1063/1.4922845>.
- ³¹R. Singh, A. Storelli, O. D. Gurcan, P. Hennequin, L. Vermare, P. Morel, and R. Singh, Plasma Physics and Controlled Fusion (accepted).
- ³²G. W. Hammett and F. W. Perkins, Phys. Rev. Lett. **64**, 3019 (Jun 1990),

<http://link.aps.org/doi/10.1103/PhysRevLett.64.3019>.

³³L. Wang and P. H. Diamond, Phys. Rev. Lett. **110**, 265006 (Jun 2013),
<http://link.aps.org/doi/10.1103/PhysRevLett.110.265006>.

³⁴L. Vermare, P. Hennequin, Ö. D. Gürçan, *et al.*, Phys. Plasmas **18**, 012306 (2011).

